



Effect of rare-earth metal ion Ce³⁺ on the structural, optical and photocatalytic properties of CdO nanoparticles

M. Elayaraja¹ · I. Kartharinal Punithavathy¹ · M. Jothibas¹ · A. Muthuvel¹ · S. Johnson Jeyakumar¹

Received: 9 August 2020 / Accepted: 14 October 2020 / Published online: 30 October 2020
© Springer Nature Switzerland AG 2020

Abstract

In this present work, effects of cerium (Ce)-doped CdO nanoparticles (NPs) were synthesized by simple chemical precipitation methods. The as-formed CdO-NPs were characterized by crystal structure (XRD), surface morphology (SEM), elemental composition (EDX), functional groups (FTIR) and optical spectroscopy (UV-DRS and PL) analysis. The XRD indicated cubic in structure of CdO-NPs that were as well crystallized with an averaged particle size of 28–33 nm. The SEM images show concise structure of CdO-NPs, and EDX spectrum revealed the presence of cerium. FTIR spectra show the fundamental peaks of CdO in the sample. The optical properties showed that the two emission peaks were recorded at 418 and 439 nm upon excited at 360 nm. The photocatalytic degradation efficiency of methyl orange dye, i.e., 93% at the optimum content of Ce³⁺-doped (5%) CdO-NPs.

Keywords Cerium · CdO-NPs · SEM · Photocatalytic activity

Introduction

Nowadays, nanomaterials such as metal oxide nanoparticles are widely used in engineering and medical science [1]. Among various metal oxides present, semiconductor nanoparticle CdO is one of the important semiconductor materials that have attracted considerable interest due to its economical, high chemical stability, optical properties and non-toxicity [2]. Because of these excellent properties, CdO-NPs are widely used for several application, such as ultraviolet lasers, photo-detectors, solar cells, light emitting diodes and photocatalytic and so on [3]. This semiconductor with direct band gap of 3.46 eV has huge exaction binding energy (60 meV) at room temperature (RT) [4]. The doping of CdO-NPs to a certain extent significantly increases surface imperfections, which may shift the absorption toward the visible region. Several research group reports noted that the role of the crystalline size, morphological, impurities, surface defects, the metal oxide host system, dopant type and dopant concentration are very important to physical and chemical

properties and various applications of CdO [5]. Recently, the effect of doing elements like Zn, Mg, Ag, Al, Tb and Ni on the electrical, optical and photocatalytic properties of CdS nanoparticles was investigated. Using Tb doping CdO-NPs synthesized via Cd hydroxychloride and effect of hydrogen post-treatment [6]. Ravichandran et al. [7] reported the optical and structural properties of Zn-doped CdO-NPs synthesized by chemical precipitation method. Jeejamol et al. [8] studied the Zr-doped CdO-NPs by chemically controlled co-precipitation method which evaluated the photocatalytic degradation of methylene blue solution. Recently, rare-earth-doped semiconductors nanoparticles have acquired interest in optical properties and environmental purification. Among them, cerium oxide has most attracted and attention for its 5*d* and 4*f* orbital functions [9]. Inserting Ce impurity inside CdO-NPs not only increases optical absorption in the visible range, but also prevents recombination and thus increases photocatalysis activities [10]. Various synthetic methods for these materials have been employed including hydrothermal/solvothermal method [11], aerosol-spraying [12], thermal evaporation [13] and co-precipitation method [14]. Among them, co-precipitation method was due to its simple and novel method and it requires a less time for synthesis. And also it has numerous advantages such as small particle size, short reaction time and well distribution with a high purity of the crystal with lower energy usage [15, 16]. In

✉ M. Jothibas
jothibas1980@gmail.com

¹ PG and Research Department of Physics, T.B.M.L. College (Affiliated To Bharathidasan University, Tiruchirappall-620024), Porayar, Tamil Nadu 609307, India

the present work, we have prepared CdO-NPs with different concentration of Ce dopant and their structural, morphological, optical and photocatalytic properties have been investigated in this paper.

Materials and methods

Chemicals

All the chemical reagents are used from analytically (AR grade) pure. Cadmium acetate dehydrate ($C_4H_6CdO_4$), cerium acetate ($Ce(CH_3COO)_2 \cdot 6H_2O$), polyethylene glycol (PEG-5000-7000) and ammonium hydroxide (NH_4OH) were obtained with 99% purity (Nice chemical company).

Synthesis of pure CdO-NPs

CdO nanoparticles were prepared by co-precipitation method. The whole synthesis is carried out in aqueous medium. 0.2 M of cadmium acetate was dissolved in 50 ml of distilled water (DW) and stirred 30 min. Then, 2% of PEG was dissolved into the above solution with constant stirring once the homogenous solution is formed. 20 ml of ammonium hydroxide solution in 50 ml of de-ionized water was dropwise added by dropper in the mixed solution. The precipitate of CdO is formed after the stirring of 5 h. The obtained precipitate was washed several times with DW and was filtered by Whatman No.1 filter paper. Subsequently, the washed precipitate was dried at 100 °C for 24 h. Finally, the product was sintering at 400 °C for 2 h in muffle Furnace. The final dried powders were taken for further characterization analysis.

Synthesis of Ce-doped CdO nanoparticles

For the synthesis of Ce-doped CdO nanoparticles, 0.2 M of cadmium acetate was dissolved in 50 ml de-ionized water and it was stirred vigorously by using magnetic stirrer, and cerium acetate of preferred percentage (1, 3, 5 and 7%) prepared in 20 ml aqueous was mixed drop by drop. 20 ml of ammonium hydroxide solution in 50 ml of de-ionized water was dropwise added by dropper in the mixed solution. Further 2% of PEG was added to the above solution. After that, mixed solution was kept stirring at room temperature (RT) for two hours. The resultant precipitant solution was washed and filtered by using de-ionized water, and then, acetone is used for washing purpose for several times. Then, the final solution was kept in hot air oven at 100 °C for 6 h for drying and then grinded by using mortar pistil to eliminate agglomerates. The resulting powder was then incubated in a muffle oven for 2 h at 400 °C to obtain the brown CdO-NPs. The

obtained samples were further powdered in an agate mortar further for characterization.

Characterizations

The crystalline phase purity of pure and cerium-doped CdO-NPs was examined by X-ray diffraction (XRD) analysis using SHIMADZU 6000 X-ray diffractometer with Cu $K\alpha$ radiation ($\lambda = 1.5406 \text{ \AA}$) at room temperature (RT). The chemical structure and functional group were examined by SHIMADZU Fourier transform infrared (FTIR) spectrophotometer where IR spectrum was used to record by mixing powder with KBr and its wavelength range is fixed 4000 and 400 cm^{-1} . Optical properties were analyzed by using JASCO V-670 spectrophotometer in the range 300–1200 nm. The surface morphology and elemental composition of the synthesized powder were examined by using SEM with EDX investigation with using JEOL JSM 6390.

Photocatalytic activity

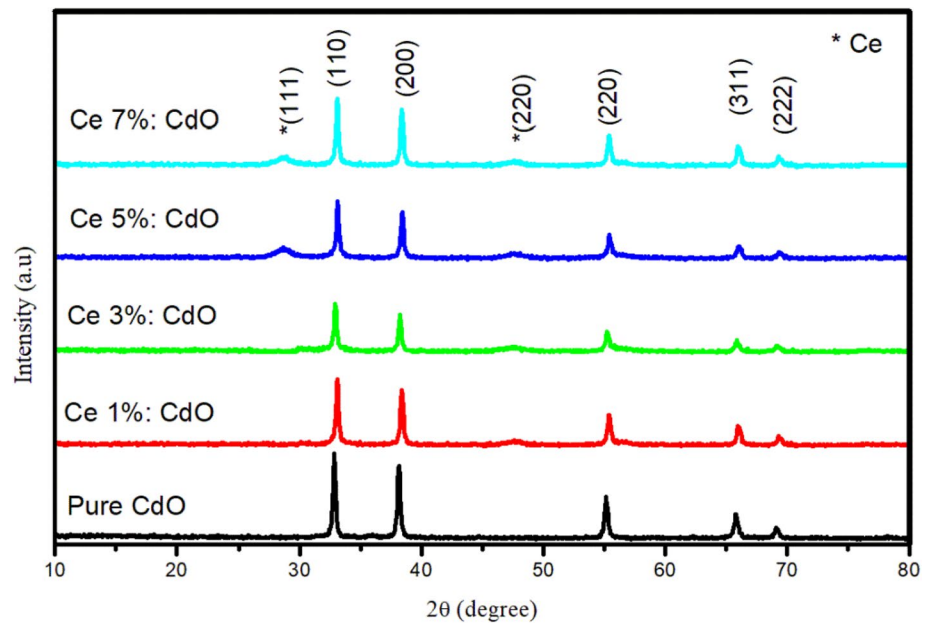
The photocatalytic activities of pure CdO and Ce-doped (5%) CdO-NPs samples were estimated by supervising photo-degradation of the methylene blue (MB) in the aqueous solution. MB was chosen because of its strong absorption, well-defined good resistance to light degradation optical absorption to metal oxide surfaces. Photocatalytic testings were carried out during sunny days from 11 am to 2 pm. The 0.06 g of photocatalyst of pure CdO was charged into 100 ml of 10 mg/l MB aqueous solution. The solution was then magnetically stirred for 30 min to attain adsorption–desorption equilibrium between dye and CdO. The solutions mixed were irradiated under sunlight. Then, solutions were taken out in every 20 min (up to 120 min) and the photocatalyst was used to separate from the solution by centrifugation, and then, the UV–visible absorption was analyzed with a UV–Vis spectrophotometer (Shimadzu, UV-1800). The maximum absorption wavelength was attained at 664 nm for the MB solution.

Results and discussion

Structural (XRD) analysis

The phase and crystallographic structure was studied by using X-ray diffraction (XRD) technique. Figure 1 demonstrates the XRD pattern of the cerium-doped CdO nanoparticle, and it is a good agreement of crystalline nature compared with standard spectra (JCPDS NO: 78-0653). The diffraction peaks in the XRD spectra of CdO-NPs occurring at 2θ values of 32°, 40°, 64°, 80° and 84° are indexed as (110), (200), (220), (311) and (222) crystal

Fig. 1 XRD spectra of pure and Ce (1, 3, 5 and 7%)-doped CdO-NPs



planes with face-centered cubic structure [17]. No diffraction peaks from cerium and no impurity peaks were detected in the samples with cerium concentration lower than 3%, representing the merging of Ce ions into the crystal lattice of CdO host. However, further increasing the Ce doping concentration up to 7%, the diffraction at 2θ values of 38.03° and 44.45° belongs to the (111), (200) crystal planes with face-centered cubic metallic cerium, which confirmed the cerium phase introduced in the CdO-NPs [17]. Compared with the pure samples, the peak intensity decreases and full-width half-maximum increases with cerium doping; results size of the doped sample decreased.

The average crystallite size, lattice parameters and dislocation density of pure and (1–7%) cerium-doped CdO-NPs calculated the following equation [18].

$$D = \frac{K\lambda}{\beta \cos \theta} \quad (1)$$

$$a = d_{hkl}(h^2 + k^2 + l^2)^{1/2} \quad (2)$$

$$\delta = \frac{1}{D^2} \text{lines/m}^2 \quad (3)$$

where K is constant (0.9), λ is the X-ray wave length (1.5405×10^{-10}), β is the full width at half maximum, and θ is the half diffraction angle. The intensity value of the (110), (200), (220), (311) and (222) planes has been found to be increasing with the increasing 1%, 3%, 5% and 7% Ce-doped CdO-NPs [19]. This result suggests that at higher 7% Ce-doped, Ce^{3+} ions replace Cd^{2+} ions in the substitution

ally. Further, the Ce^{3+} -ions incorporated in the lattice are interstitial sites in the CdO-NPs. The XRD intensity depends strongly on the allowed cerium concentration. The maximal intensity of XRD spectra is illustrated by the pronounced peak with doping content. The similar result was observed Moholkar et al. [20].

It is shown that the decrease in crystal size is correlated with the broadening of the XRD peak. The smaller crystal size results in higher densities of grain boundaries, which act as barriers to carrier grain boundaries, carrier transport and trapping for free carriers. Therefore, decreasing the crystal size will increase the grain boundary scattering [21]. The lattice parameters for the face-centered cubic structure of pure and Ce-doped CdO-NPs were calculated by the following equation [22]. The lattice constant of pure and Ce-doped CdO nanoparticles was calculated using the relevant formula and systematically represented in Table 1. The variation of lattice constant with Ce doping shown in table, where the lattice constant decreases, reaches a minimum value around (\AA) a pure CdO nanoparticles and then slowly increased with increase in doping around 4.921–4.016 \AA . The slight change in lattice constant for the preparation of Ce-doped CdO nanoparticles over bulk clearly suggests that the particles are strained, which may be due to the nature and concentration of the native imperfection changing. The variation of the percentage of the cerium in the cadmium oxide is associated with the changing in grain and grain boundary. The dislocation density represents length of dislocation lines per unit volume in the crystal. Larger D and smaller δ values indicate better crystallization of the particles. Dislocation density exhibits a decrease with increase in percentages, which indicate that the higher doping percentage reduces

Table 1 Observed different parameters of pure and Ce-doped CdO nanoparticles from XRD

Sample (%)	Crystal size (D) nm	2θ ($^\circ$)	Micro-strain $\epsilon \times 10^{-3}$	Dislocation density $\times 10^{14}$ (1/m ²)	Lattice constant (\AA)
Pure	33.54	33.0454	1.047	8.8894	4.691
1	32.12	33.0453	1.102	9.5819	4.686
3	30.75	33.0649	1.121	9.6451	4.684
5	28.03	33.0946	1.087	9.8457	4.678
7	30.05	33.0612	1.113	9.5994	4.671

Table 2 Comparison of crystalline size and band gap energy of Ce-doped CdO-NPs from Ce-doped other semiconductor materials

Materials used	Crystalline size (nm)	Band gap (eV)	References
Ce:CdO-NPs	28.03	2.53	Present work
Ce:ZnO-NPs	74.00	3.18	[23]
Ce:MgO-NPs	23.00	3.22	[24]
Ce:TiO ₂ -NPs	16.01	2.2	[25]
Ce:ZnS-NPs	–	3.97	[26]
Ce: Fe ₂ O ₃ -NPs	40	1.63	[27]

the crystal lattice imperfections. This result suggests that Ce (7%)-doped CdO-NPs shows the high level of surface defects in crystal quality and low level of surface defects and good crystal quality obtained for Ce (1%, 3% and 5%) CdO-NPs. These results are compared to the other Ce-doped materials as shown in Table 2

XPS analysis

Figure 2 shows the typical XPS spectrum of Ce (5%)-doped CdO-NPs. Wide scan of XPS spectra shown in Fig. 2a exhibited Cd and O peaks and hence sustained the chemical purity of the surface of Ce-doped CdO-NPs. Figure 2b, c shows the high-resolution XPS spectra of the elements Cd and O, respectively. Figure 2a shows the XPS spectrum of Ce-doped CdO-NPs; the Cd 3d features consist of the major 3d_{5/2} (405 eV) and 3d_{3/2} (412 eV) spin-orbit components, along with the features Cd 4d_{5/2} (10.5 eV), Cd 4d_{3/2} (11.5 eV), Cd 4p_{3/2} (64.2 eV), Cd 4p_{1/2} (65.7 eV), Cd 4s (110.6 eV), Cd 3p_{3/2} (620.2 eV), Cd 3p_{1/2} (654.9 eV) and Cd 3s (776.4 eV) [28]. Figure 2b shows that the two strong peaks corresponding to Cd 3d_{5/2} and Cd 3d_{3/2} for the native oxide were found to be 6.4 eV for Ce-doped CdO-NPs, which coincide extremely well with that reported for CdO [29]. In doping, Cd 3d features from the XPS spectrum appear to be suppressed due to the conversion of Cd²⁺ by

the dopant ions in the host lattice. The broad O 1s peak of Ce-doped CdO-NPs is resolved as a component centered at 521.7 eV, with oxygen adsorbed at the surface, O²⁻ ions in the CdO lattice and oxygen deficient areas, respectively [28]. Figure 4c shows that the broad O 1s peak of Ce-doped CdO-NPs is resolved into one component centered at 524.6 eV, corresponding to adsorbed oxygen on surface, O²⁻ ions in CdO lattice and the oxygen deficient regions, respectively. According to previous reports, they emerged from surface defects and chemical oxygen, respectively [30].

Functional group (FTIR) analysis

FTIR spectra of pure and Ce (1, 3, 5 and 7%)-doped CdO-NPs are shown in Fig. 3. The pure CdO-NPs show absorption peaks at 3465.68, 2348.76, 1649.32, 1418.00 and 514.46 cm⁻¹. The peak at 3465.68 and 2348.76 cm⁻¹ is corresponded to hydroxyl (OH) stretching of water and the presence of C–H symmetric stretching [31]. The band around 1649.32 cm⁻¹ can be assigned to the O–H–O bending vibration, respectively [32]. The absorption band at 1418.00 cm⁻¹ confirms the deformation vibration of the C–H of alkane group [31]. The most intense wide observed absorption band at 514.46 cm⁻¹ is attributed to the stretching of vibration of CdO.

The different percentage (1, 3, 5 and 7%) of Ce-doped CdO-NPs for the FTIR spectra shows characterized absorption bands around 3450–3400 cm⁻¹, 1650–1600 cm⁻¹, 1450–1400 cm⁻¹ and 550–500 cm⁻¹. The absorption band around 3450–3400 cm⁻¹ may be due to symmetrical stretching vibration bands of H₂O molecules, respectively [33]. The band around 1650–1600 cm⁻¹ may correspond to stretching vibrations of primary and secondary amines [31]. The specified weak band around at 1450–1400 cm⁻¹ is assigned to C–O stretching vibrations of the carbonyl group, respectively [10]. The band around 550–500 cm⁻¹ represents the Cd–O phase [7]. From the graph, it is observed that the no additional peak and some of the peak position in Ce-doped CdO-NPs are slightly shifted toward higher wavenumbers when compared to that of pure CdO-NPs. The shift is due to an interaction of Ce ions with CdO-NPs which indicates the decrease optical band gap and crystalline size values [11].

Morphology and elemental (SEM with EDAX) analysis

The surface morphology of pure and Ce (5%)-doped CdO-NPs examined by scanning electron microscopy (SEM) is shown in Fig. 4. The resulting microstructure exhibited a uniform and concise structure interconnected by grains (Fig. 4a1, b1). The particles sizes are found to be 31 nm and 26 nm for pure and Ce-doped CdO-NPs, respectively (Fig. 4a3, b3). The particles size of the Ce-doped CdO-NPs

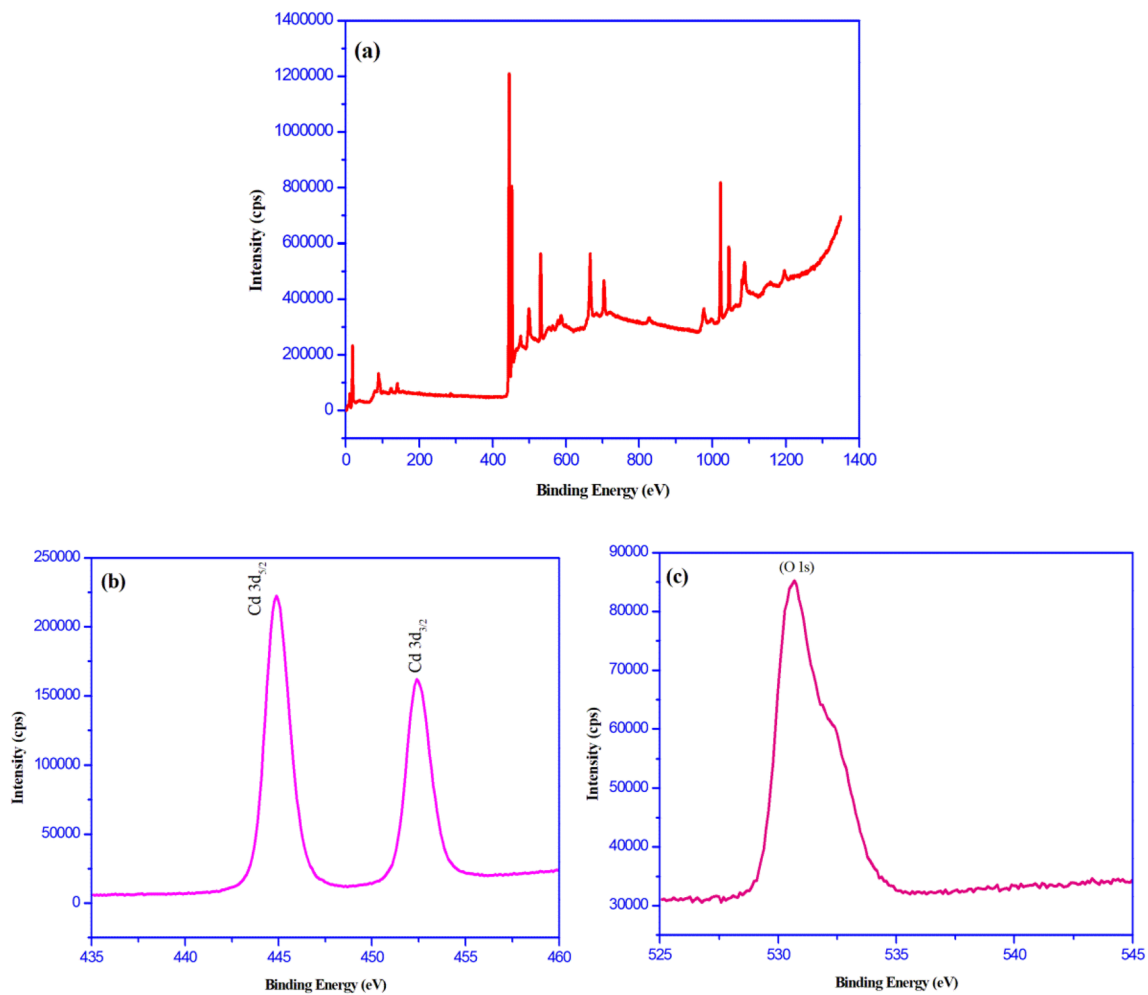


Fig. 2 XPS spectrum of Ce (5%)-doped CdO-NPs

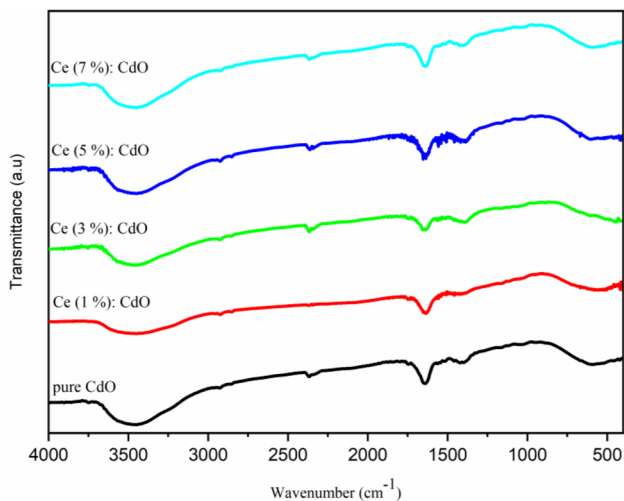


Fig. 3 FTIR spectra of pure and Ce (1, 3, 5 and 7%)-doped CdO nanoparticles

is found to be reduced as compared to that of pure CdO-NPs. This reduction in particle size is due to the distortion in the host material incorporated with Ce^{3+} metal ion in CdO-NPs surface area. Hence, the size of CdO-NPs is reduced by Ce doping. EDAX spectra verified the presence of Cd, O and Ce in the doped CdO nanostructure. The peak corresponding to Cd, O and Ce elements located their normal energy (Fig. 4 A2 and B2).

Optical analysis

UV–Vis spectroscopy is a powerful nondestructive method for realizing optical properties of semiconducting nanoparticles [34]. The absorption spectra of CdO nanoparticles were analyzed in the UV–Vis spectra. Figure 5 shows the obtained UV–Vis spectra of pure and Ce (1–7%)-doped CdO-NPs. From Fig. 5, the absorption peaks locate at 242, 245, 247, 249, 250 and 252 nm pure and Ce-doped CdO-NPs, respectively. A dissimilar blue shift was observed in the

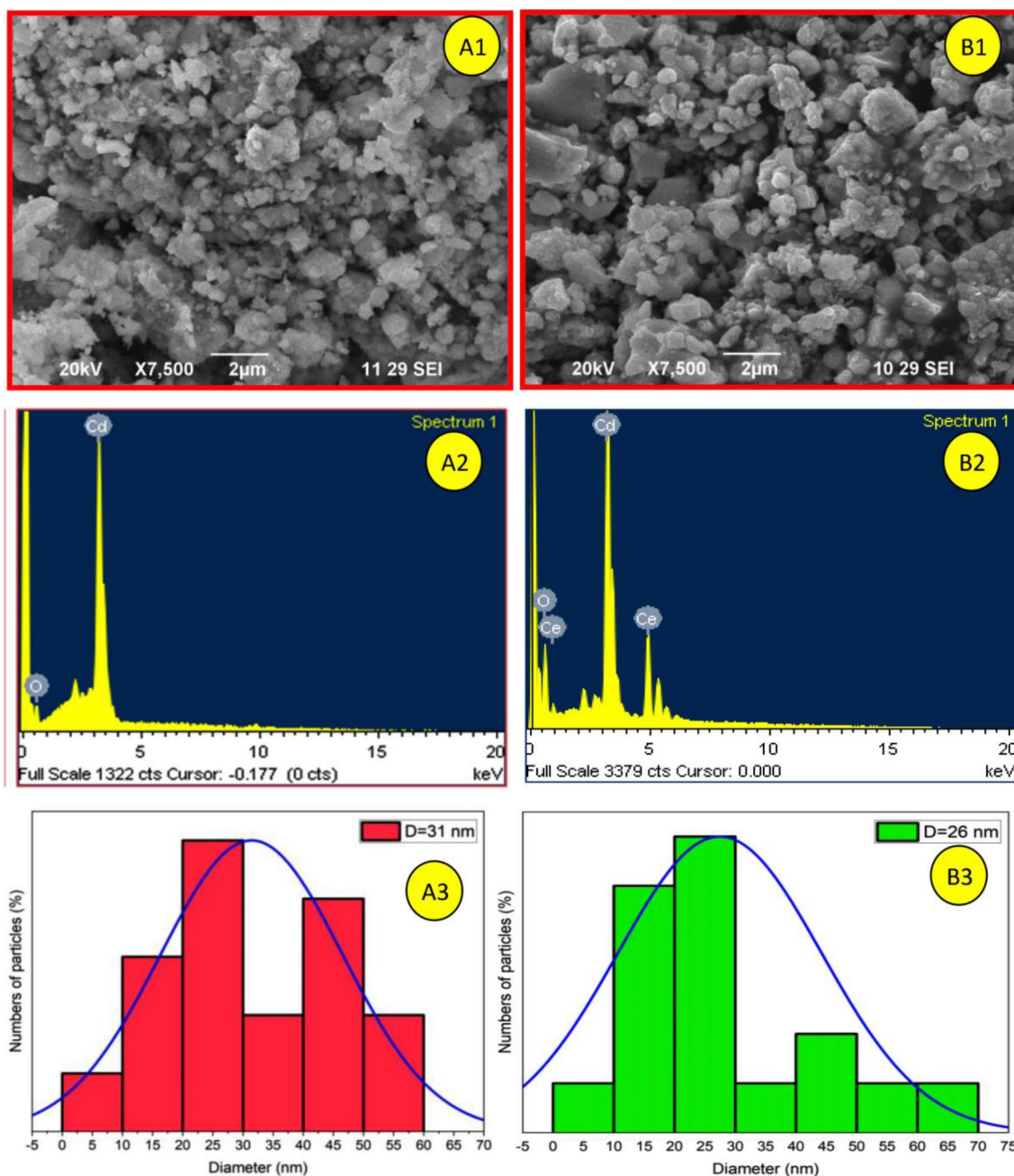


Fig. 4 A1-B1 SEM image; A2-B2 EDAX spectra; A3-B3 particle size histogram of pure and Ce (5%)-doped CdO-NPs

absorption edges for the Ce-doped CdO-NPs as comparison of pure. The observed blue shift points out a minor variation in the band structure in the Ce-doped CdO-NPs due to the incorporation of Ce ions [35]. The optical band gap (E_g) is determined from a Tauc plot from the following relation [36]

$$\alpha = \frac{A(h\nu - E_g)^{1/2}}{h\nu} \tag{4}$$

where α is absorption coefficient, h is planks constant, ν is the frequency of light radiation, and E_g is the band gap energy, where ‘ n ’ takes the value of $1/2$ for allowed direct transition. The band gap energies are negative number for $n=2, 3/2$ and 3 ; hence, relationship fitting to the CdO is $n=1/2$, which confirms the allowed direct transition. Figure 6 shows the curves of $(ah\nu)^2$ versus $h\nu$ for pure and Ce-doped CdO nanoparticles prepared with different doping percentage. The E_g values were obtained by extrapolating the straight line portions of the graph to the X-axis. From the

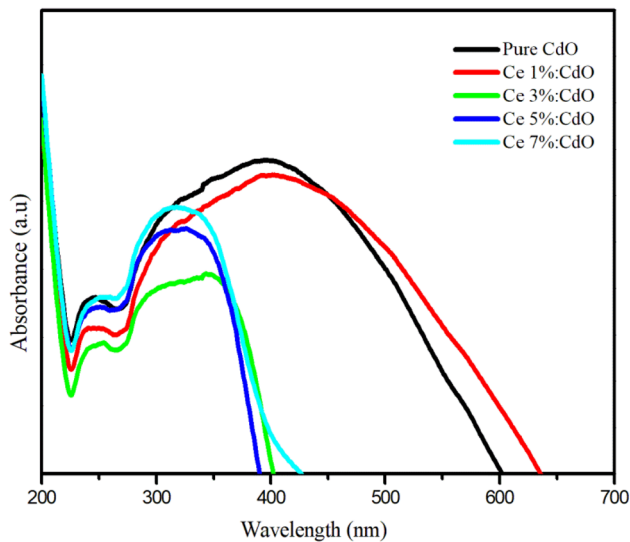


Fig. 5 UV-Vis spectra of pure and Ce (1, 3, 5 and 7%)-doped CdO nanoparticles

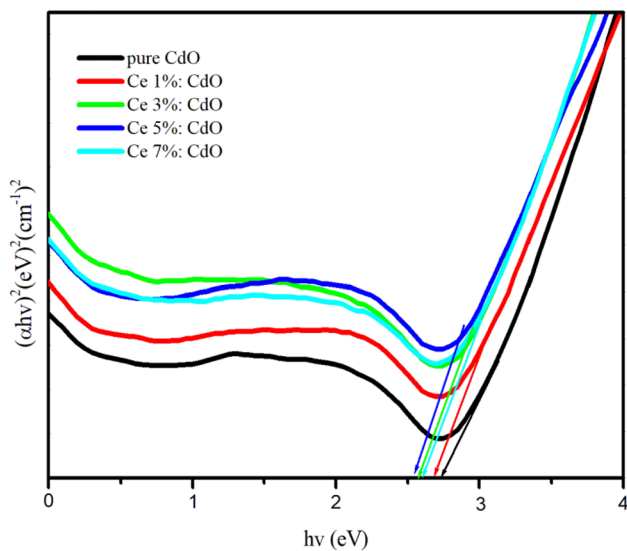


Fig. 6 Optical band gap spectra of pure and Ce (1, 3, 5 and 7%)-doped CdO nanoparticles

figure, the band gap energy for pure and different percentage (1, 3, 5 and 7%) of Ce-doped CdO-NPs is 2.69, 2.64, 2.60, 2.53 and 2.58 eV, respectively. It can be seen that the band gap of the Ce-doped CdO-NPs was lower than that the pure CdO-NPs. The optical band gap energy decreases as the percentage of Ce ions increases from 1 to 5%, and further increase in the Ce (7%) percentage also increases the optical band gap energy due to strong quantum confinement's effect [37]. The band gap energy decreases which (Table 3) confirms the presence of Ce^{3+} inside the CdO-NPs. Furthermore, the ions in the CdO can form a new energy band,

Table 3 Band gap energy of pure and Ce-doped CdO nanoparticles

Sample (%)	Band gap (eV)
Pure	2.69
Ce 1%-doped CdO	2.64
Ce 3%-doped CdO	2.60
Ce 5%-doped CdO	2.53
Ce 7%-doped CdO	2.58

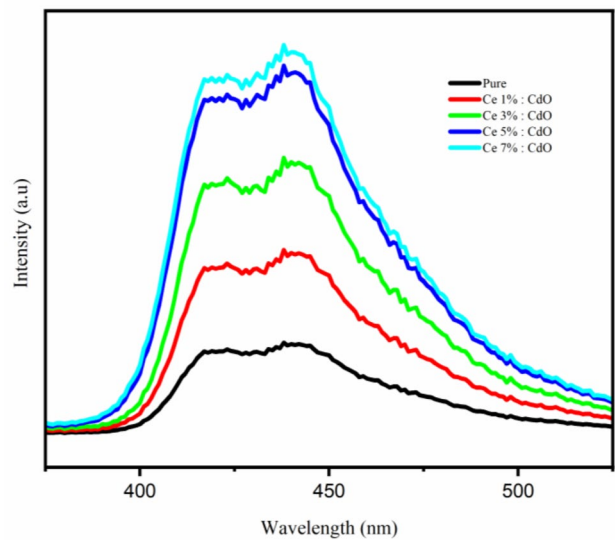


Fig. 7 PL spectra of pure and Ce (1, 3, 5 and 7%)-doped CdO nanoparticles

which means that the impurity band overlaps with the band gap of the pure CdO, resulting in the band gap. This effect is called band gap shortening. This shortening of the band gap for Ce-doped CdO-NPs compared to the CdO indicates the transfer of C ions to the Cd sites in the CdO. This may also be due to an increase in number of defects in Ce content. This result suggests that the doping of Ce into the host CdO lattice be able to effectively tailor the energy band. The variation of band gap found in our samples could have the promising future scope in the field of photo-catalytic applications.

Photoluminescence spectroscopy (PL) studies

Photoluminescence spectroscopy study is an effective technique to examine the occurrence of defects in the semiconductors. The PL spectra of our pure and Ce-doped CdO-NPs recorded at RT are shown in Fig. 7. The appearance of two different peaks with Gaussian Function was attaining for all PL spectra. The near-band-edge emissions were observed at 418 and 439 nm for pure and Ce-doped CdO-NPs, and are attributed to recombination of free

exciton–exciton collision process [38]. The violet emission centers at 418 nm for pure and Ce-doped CdO-NPs are due to its electron transition from shallow donor level of neutral Ce to the valence band [39]. Finally, the blue emission wavelength of 439 nm for pure and all Ce doped CdO-NPs illustrates the transition in-between oxygen vacancy and oxygen interstitial defects [6]. This change of the emission confirms the substitution of Ce^{3+} ions into CdO-NPs. The increase in Ce percentage is associated with structural disorganization level, and the charge transfer occurred between cadmium, cerium and oxygen ions. The raise in Ce percentage significantly decreases the band gap up to 5% which allows faster recombination of electron in Cd and Ce conduction bands with holes in oxygen valence band by increasing PL intensity.

Photocatalytic activities

The photocatalytic activities of pure and Ce-doped CdO-NPs were evaluated by decomposing aqueous methylene blue (MB). Figure 8a, b exhibits the change in absorption pattern of MB exposed to UV-light for various irradiation times in the presence of CdO and Ce-doped CdO-NPs, respectively, percentage of the degradation was calculated, and the results are given Table 4. As seen from Fig. 8, the intensity of absorption peaks decreases with increase in time intervals. The occurrence of catalytic activity under UV and Vis irradiation result shows that the photocatalytic degradation of Ce-doped CdO-NPs is 93.58% of efficiency at 120 min under sunlight. Thus, greater photocatalytic degradation efficiency was achieved in short period in the case-doped sample when compared to pure CdO, which means that the number of active surface siter increases as the grain size decreases, and hence, it enhances the photocatalytic activity.

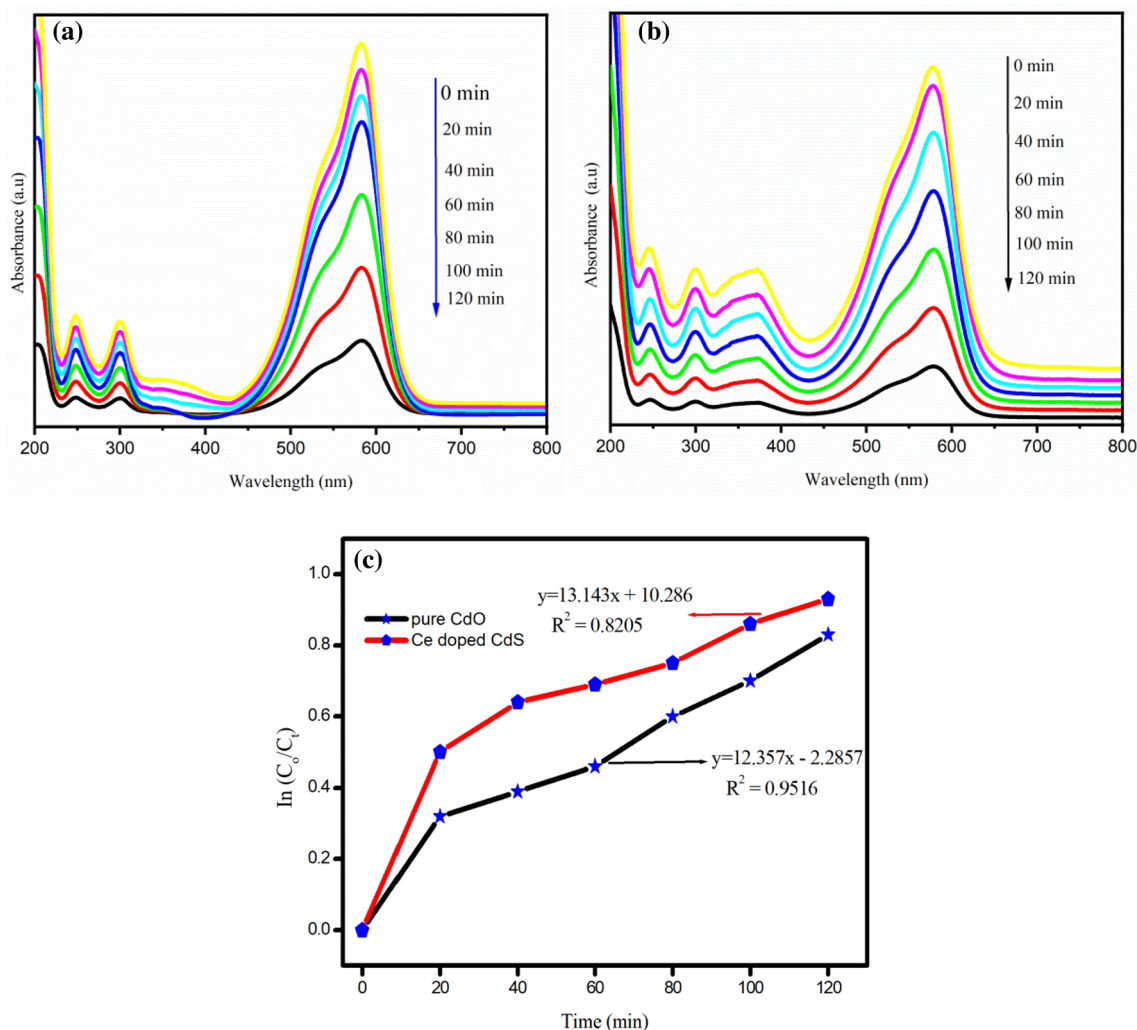


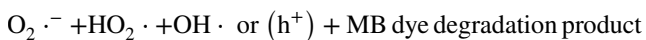
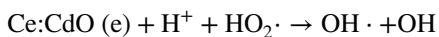
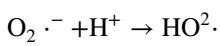
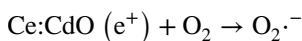
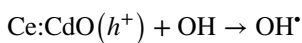
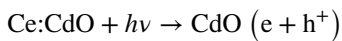
Fig. 8 a, b UV–Vis absorption spectra of MB with respect to irradiation time, c first-order kinetics of the pure and Ce (5%)-doped CdO-NPs

Table 4 The effect of MB dye degradation of pure and Ce (5%)-doped CdO-NPs

Time (min)	% of degradation of MB dye	
	Pure CdO	Ce-doped CdO
0	0	0
20	32.12	50.66
40	39.86	64.17
60	46.14	69.51
80	60.23	75.32
100	70.18	89.52
120	83.21	93.58

Mechanism of photocatalytic activity

The possible mechanism of improved photo-catalytic activity of Ce-doped CdO-NPs is explained [40];



When the lights of energy are greater than the forbidden gap, irradiated electrons from the valance band can make a quantum jump to conduction band of CdO. The presence of dopant Ce^{3+} within crystal matrix/surface of CdO can trap the photo-generated electrons/holes and consequently transfers the same to adsorbed oxygen and the hydroxyl ions to generate super oxide radicals ($\text{O}_2^{\bullet-}$) and hydroxide radicals (OH^\bullet), respectively; this behavior will reduce electron. Hence, recombination and generates are more and more free radicals responsible for the degradation of MB dye. In this way, Ce doped CdO-NPs exhibit better activity for the degradation of dye methylene blue.

Kinetic study

These smaller grains can enhance the photocatalytic activity for the degradation of dye; further rate constant for dye degradation of the catalysis was calculated using the first-order rate equation [41];

$$\ln \frac{C_0}{C_t} = kt \quad (5)$$

where K is the first-order rate constant, Fig. 8c shows the plot depicting liner relationship between $\ln \frac{C_0}{C_t}$ and time for all samples and slope of the graph, and rate constant values were calculated. The value of rate constant for CdO was found to be 0.01234 min^{-1} , whereas, for Ce-doped CdO-NPs, it was increased to 0.02143 min^{-1} , and the increased K values suggest the improved photo-catalytic activity of Ce-doped CdO-NPs. The possible mechanism of improved photocatalytic activity of Ce-doped CdO-NPs is explained.

Conclusions

The effect of cerium doping at different percentages on the structural, optical and morphological properties of pure and Ce-doped CdO nanoparticles synthesized by co-precipitation method has been studied. Structural studies show that the particles are polycrystalline nature with cubic structure. Surface morphology reveals that the particles are uniform with spherical shaped grains appeared on the surface. The optical band gap value decreased with increase in doping percentages. Based on the above results, it is concluded that the pure and cerium-doped cadmium oxide nanoparticles have exhibited suitability for a potential candidate for addressing the environmental pollution caused by organic dyes.

Compliance with ethical standards

Conflict of interest The authors declare that they have no conflict of interest.

References

1. Afzalian Mend B, Delavar M, Darroudi M (2017) CdO-NPs; synthesis from 1D new nano Cd coordination polymer, characterization and application as anti-cancer drug for reducing the viability of cancer cells. *J Mol Struct* 1134:599–605
2. Dabour K, Al Naggar Y, Masry S, Naiem E, Giesy JP (2019) Cellular alterations in midgut cells of honey bee workers (*Apis mellifera* L.) exposed to sublethal concentrations of CdO or PbO nanoparticles or their binary mixture. *Sci Total Environ* 651:1356–1367
3. Chen Z-Y, Abdelhamid HN, Wu H-F (2016) Effect of surface capping of quantum dots (CdTe) on proteomics. *Rapid Commun Mass Spectrom* 30(12):1403–1412
4. Nagabhushana H, Basavaraj RB, Daruka Prasad B, Sharma SC, Premkumar HB, Vijayakumar GR (2016) Facile EGCG assisted green synthesis of raspberry shaped CdO nanoparticles. *J Alloys Compd* 669:232–239
5. Abdelhamid HN, Chen Z-Y, Wu H-F (2017) Surface tuning laser desorption/ionization mass spectrometry (STLDI-MS) for the

- analysis of small molecules using quantum dots. *Anal Bioanal Chem* 409(21):4943–4950
6. Dakhel AA (2016) Defect-induced ferromagnetic properties of Tb-doped CdO synthesized via Cd hydroxychloride: effect of hydrogen post treatment. *Mater Res* 19(2):379–383
 7. Ravichandran AT, Robert Xavier A, Pushpanathan K, Nagabhushana BM, Chandramohan R (2015) Structural and optical properties of Zn doped CdO nanoparticles synthesized by chemical precipitation method. *J Mater Sci Mater Electron* 27(3):2693–2700
 8. Jeejamol DJ, Raj AME, Jayakumari K, Ravidhas C (2017) Optimization of CdO nanoparticles by Zr⁴⁺ doping for better photocatalytic activity. *J Mater Sci Mater Electron* 29(1):97–116
 9. Abdelhamid HN, El-Bery HM, Metwally AA, Elshazly M, Hathout RM (2019) Synthesis of CdS-modified chitosan quantum dots for the drug delivery of Sesamol. *Carbohydr Polym* 214:90–99
 10. Sankarasubramanian K, Babu KJ, Soundarajan P, Logu T, Gnana-kumar G, Ramamurthi K, Sethuraman K, Senthil Kumar SM (2019) A new catalyst Ti doped CdO thin film for non-enzymatic hydrogen peroxide sensor application. *Sens Actuat B Chem* 285:164–172
 11. Zeid EFA, Ibrahim IA, Ali AM, Mohamed WAA (2019) The effect of CdO content on the crystal structure, surface morphology, optical properties and photocatalytic efficiency of p-NiO/n-CdO nanocomposite. *Results Phys* 12:562–570
 12. Eskandari A, Jamali-Sheini F (2018) Sonochemical synthesis of Cu-doped CdO nanostructures and investigation of their physical properties. *Mater Sci Semicond Process* 74:210–217
 13. Yousef A, Barakat NAM, Al-Deyab SS, Nirmala R, Pant B, Kim HY (2012) Encapsulation of CdO/ZnO NPs in PU electrospun nanofibers as novel strategy for effective immobilization of the photocatalysts. *Colloids Surf A* 401:8–16
 14. Kahane SV, Sasikala R, Vishwanadh B, Sudarsan V, Mahamuni S (2013) CdO–CdS nanocomposites with enhanced photocatalytic activity for hydrogen generation from water. *Int J Hydrogen Energy* 38(35):15012–15018
 15. Abdelhamid HN (2020) High performance and ultrafast reduction of 4-nitrophenol using metal-organic frameworks. *J Environ Chem Eng*. <https://doi.org/10.1016/j.jece.2020.104404>
 16. Kassem AA, Abdelhamid HN, Fouad DM, Ibrahim SA (2020) Hydrogenation reduction of dyes using metal-organic framework-derived CuO@C. *Microporous Mesoporous Mater* 305:110340
 17. Sabri NS, Deni MSM, Zakaria A, Talari MK (2012) Effect of Mn doping on structural and optical properties of SnO₂ nanoparticles prepared by mechanochemical processing. *Phys Procedia* 25:233–239
 18. Muthuvel A, Jothibas M, Manoharan C, Jayakumar SJ (2020) Synthesis of CeO₂-NPs by chemical and biological methods and their photocatalytic, antibacterial and in vitro antioxidant activity. *Res Chem Intermed* 46(5):2705–2729
 19. Sudheer Khan S (2015) Enhancement of visible light photocatalytic activity of CdO modified ZnO nanohybrid particles. *J Photochem Photobiol B* 142:1–7
 20. Venkatesu P (2013) Doping effect of Mn on structural optical magnetic and electrical properties of CdS nanoparticles. In: International conference on advanced nanomaterials and emerging engineering technologies
 21. Gupta VK, Fakhri A, Tahami S, Agarwal S (2017) Zn doped CdO nanoparticles: structural, morphological, optical, photocatalytic and anti-bacterial properties. *J Colloid Interface Sci* 504:164–170
 22. Mourdikoudis S, Pallares RM, Thanh NTK (2018) Characterization techniques for nanoparticles: comparison and complementarity upon studying nanoparticle properties. *Nanoscale* 10(27):12871–12934
 23. Aisah N, Gustiono D, Fauzia V, Sugihartono I, Nuryadi R (2017) Synthesis and enhanced photocatalytic activity of Ce-doped zinc oxide nanorods by hydrothermal method. In: IOP conference series: materials science and engineering, vol 172. pp 012037
 24. Srisuvetha VT, Rayar SL, Shanthy G (2020) Role of cerium (Ce) dopant on structural, optical and photocatalytic properties of MgO nanoparticles by wet chemical route. *J Mater Sci Mater Electron* 31(4):2799–2808
 25. Hou T, Mao J, Zhu X, Tu M (2006) STM and STS investigations of Ce-doped TiO₂ nanoparticles. *Rare Met* 25(4):331–336
 26. Anand KV, Mohan R, Kumar RM, Chinnu MK, Jayavel R (2011) Controlled synthesis and characterization of cerium-doped zns nanoparticles in hmta matrix. *Int J Nanosci* 10(03):487–493
 27. Cardillo D, Konstantinov K, Devers T (2013) The effects of cerium doping on the size, morphology, and optical properties of α-hematite nanoparticles for ultraviolet filtration. *Mater Res Bull* 48(11):4521–4525
 28. Zhang J, Gao D, Yang G, Zhang J, Shi Z, Zhang Z, Zhu Z, Xue D (2011) Synthesis and magnetic properties of Zr doped ZnO Nanoparticles. *Nanoscale Res Lett* 6(1):587
 29. Gulino A, Castelli F, Dapporto P, Rossi P, Fragalà I (2002) Synthesis and characterization of thin films of cadmium oxide. *Chem Mater* 14(2):704–709
 30. Poulouse AC, Veeranarayanan S, Yoshida Y, Maekawa T, Kumar S (2012) Rapid synthesis of triangular CdS nanocrystals without any trap emission. *J Nanoparticle Res* 14(4):789. <https://doi.org/10.1007/s11051-012-0789-5>
 31. Xue Y, Luan Q, Yang D, Yao X, Zhou K (2011) Direct evidence for hydroxyl radical scavenging activity of cerium oxide nanoparticles. *J Phys Chem C* 115(11):4433–4438
 32. Muthuvel A, Jothibas M, Manoharan C (2020) Synthesis of copper oxide nanoparticles by chemical and biogenic methods: photocatalytic degradation and in vitro antioxidant activity. *Nanotechnol Environ Eng* 5(2). <https://doi.org/10.1007/s41204-020-00078-w>
 33. Bomila R, Srinivasan S, Venkatesan A, Bharath B, Perinbam K (2017) Structural, optical and antibacterial activity studies of Ce-doped ZnO nanoparticles prepared by wet-chemical method. *Mater Res Innov* 22(7):379–386. <https://doi.org/10.1080/14328917.2017.1324379>
 34. Jafari A, Khademi S, Farahmandjou M (2018) Nano-crystalline Ce-doped TiO₂ powders: sol-gel synthesis and optoelectronic properties. *Mater Res Express* 5(9):095008
 35. Kumar N, Misra KP, Jain SK, Choudhary BL (2013) Structural and morphological properties of Ce doped ZnO. *AIP Conf Proc* 1536(1). <https://doi.org/10.1063/1.4810372>
 36. Muthuvel A, Jothibas M, Mohana V, Manoharan C (2020) Green synthesis of cerium oxide nanoparticles using *Calotropis procera* flower extract and their photocatalytic degradation and antibacterial activity. *Inorg Chem Commun* 119:108086
 37. Ramasamy V, Mohana V, Rajendran V (2018) Characterization of Ca doped CeO₂ quantum dots and their applications in photocatalytic degradation. *OpenNano* 3:38–47
 38. Culik F (1966) Exciton-exciton ‘collisions’ in crystals. *Czech J Phys* 16(3):194–206
 39. Zeng H, Duan G, Li Y, Yang S, Xu X, Cai W (2010) Blue luminescence of ZnO nanoparticles based on non-equilibrium processes: defect origins and emission controls. *Adv Func Mater* 20(4):561–572
 40. Kumar S, Ojha AK, Walkenfort B (2016) Cadmium oxide nanoparticles grown in situ on reduced graphene oxide for enhanced photocatalytic degradation of methylene blue dye under ultraviolet irradiation. *J Photochem Photobiol B* 159:111–119
 41. Muthuvel A, Jothibas M, Manoharan C (2020) Effect of chemically synthesis compared to biosynthesized ZnO-NPs using *Solanum nigrum* leaf extract and their photocatalytic, antibacterial and in vitro antioxidant activity. *J Environ Chem Eng* 8(2):103705

Publisher's Note Springer Nature remains neutral with regard to jurisdictional claims in published maps and institutional affiliations.